Meccanica (2021) 56:3079–3096
https://doi.org/10.1007/s11012-021-01432-1

A node-to-surface linear complementarity problem approach for general three-dimensional contact analysis

Chu Zhang · Huimin Dong · Chuang Zhang · Delun Wang · Shudong Yu

Received: 18 January 2021 / Accepted: 21 September 2021 / Published online: 5 November 2021

Abstract Contact between two deformable bodies is a complex nonlinear problem especially when rigid-body motion and geometric errors of components are taken into consideration. In this paper, an effective node-to-surface contact scheme, termed as NTS-LCP, is presented to handle three-dimensional quasi-static contact between deformable bodies experiencing prescribed rigid body motion. The scheme is developed on the basis of the finite element modelling and the component substructuring, and formulated as a linear complementarity problem (LCP) for a speedy and robust solution to the gap sizes and contact forces by means of the well-known Lemke algorithm. The proposed scheme is valid for both conforming and non-conforming meshes. The accuracy and efficiency of the proposed scheme were established through two test cases—cam-follower contact and gear-gear contact, and comparisons with the ANSYS benchmark solution and the Hertz contact theory. The proposed scheme, effective and versatile, is successfully implemented in a computer code to investigate the effects of gear tooth modifications and assembly errors on transmission characteristics of spur gears and helical gears. It is anticipated that the results reported in the paper are useful in design of mechanical systems for optimal performance.

Keywords Contact · Finite element method · Gear pairs · Linear complementarity problem · Node-to-surface contact elements · Substructuring

C. Zhang · H. Dong (✉) · C. Zhang · D. Wang
School of Mechanical Engineering, Dalian University of Technology, Dalian, China
e-mail: donghm@dlut.edu.cn

S. Yu
Department of Mechanical and Industrial Engineering, Ryerson University, Toronto, Canada

1 Introduction

Contact between two deformable bodies is commonly encountered in mechanical systems. Examples include contact between two links at a joint, between cam and follower, between mating gears, and between rollers and races in bearings. Accurate modeling of contact is important in understanding the static and dynamic behaviors of mechanical systems involving contact.

The Hertz contact theory and various schemes [1–24] have been employed for contact between deformable bodies. The classical Hertz contact method, computationally efficient in handling contact between non-conforming bodies, has found wide applications in gear drives, bearings, cams, and joints [2–10]. In dealing with contacting bodies with geometric errors, the finite element method is often used to model the deformations of contacting bodies with desired accuracy and solve the multi-body contact problem in connection with the trial-and-error scheme [11], the nonlinear iteration scheme [12], or

the LCP scheme [13, 14]. Although the trial-and-error scheme and the nonlinear iteration scheme can be conveniently implemented and programmed, it is tedious to solve the nonlinear contact problems for which the convergence is not always guaranteed. In this paper, at a prescribed system configuration, a judicial transformation is used to convert the nonlinear contact problem into an LCP for which a robust mathematical programming method such as the Lemke algorithm [14] can be used to find a solution effectively for all potential contact pairs.

Contact between two bodies is treated as interactions between the potential contact surfaces belonging to two different bodies, referred to as the contactor surface and the target surface in the contact mechanics community. Through proper discretization of the contacting bodies and their potential contacting surfaces, a node-to-node contact scheme or a node-to-surface contact scheme can be developed [15–19].

The contact constraints for the node-to-node contact elements are satisfied in the direction from the contactor nodes to the target nodes. The node-to-node contact scheme is suitable for conforming meshes. As a result, re-meshing is required to transform the non-conforming meshes into conforming meshes with the aid of variable-node elements [15, 16] or mesh refinement method [20, 21]. The node-to-node based LCP scheme has been used by some scholars to deal with contact problems including gear-to-gear contact [22–28].

For a node-to-surface (NTS) contact element, the contact constraint is established by the contact force between the contactor nodes and its potential contact surface element [17, 18]. The NTS contact elements, suited for conforming and non-conforming meshes [15], can be used to deal with general contact problems without re-meshing [19]. In addition, it is feasible to model the geometric errors of contact surfaces. In the literatures [15–19], the contact constraints of the NTS contact elements are handled with the nonlinear iteration scheme [12]. To achieve guaranteed robustness and accuracy, formulation of the contact problem into an LCP is desired. With the help of component substructuring [29] and reduction of the non-contact related interior degrees of freedom (DOFs), a very efficient contact procedure involving only the contact related DOFs is developed.

For the practical engineering application, the gear-to-gear contact with rigid-body motion and geometric errors is a complex nonlinear problem, which requires high accuracy and high computational speed. Tooth modifications, beneficial for improving the contact performance, can be handled through the introduction of geometric errors to the finite element model of gears. This inspires the authors to analyze the gear-to-gear contact performance as a case study to validate the effectiveness and versatility of the proposed NTS-LCP scheme.

In this paper, the NTS-LCP scheme is implemented into a computer code by combining the finite element modeling and component substructuring with LCP formulating between the paired gap sizes and contact forces for all NTS contact elements as complementarity variables, for simulating quasi-static contact between two deformable bodies. Numerical results were obtained using the proposed scheme and compared with those of ANSYS for the cam-follower contact and gear-to-gear contact. Good agreement was achieved. The effects of tooth modifications and assembly errors on gear contact characteristics were further investigated through series of parametric studies.

2 Description of NTS-LCP scheme

2.1 Problem description

Figure 1 shows two bodies in contact at a prescribed configuration. The target body is properly constrained against any rigid body motion under load. The contactor body can experience both rigid body displacements and elastic deformations. The surfaces of potential contact on the contactor and target bodies can be determined by the kinematic geometry. A node on the contactor body is considered to associate with a small surface on the target body. An NTS contact element, shown in Fig. 1 is defined as the paired contactor node and a four-node target surface element.

It is noted that the actual point of contact under loads is unknown a priori. To formulate contact as a linear complementarity problem, it is hypothesized that the contact constraint between a contactor node o_k and its associated target surface element is enforced along the direction $\boldsymbol{n}_k$, the unit vector from o_k to p_k, where p_k is the point on the target surface element such that $o_k p_k$ is the minimum distance between o_k and the target element. The actual direction of contact may

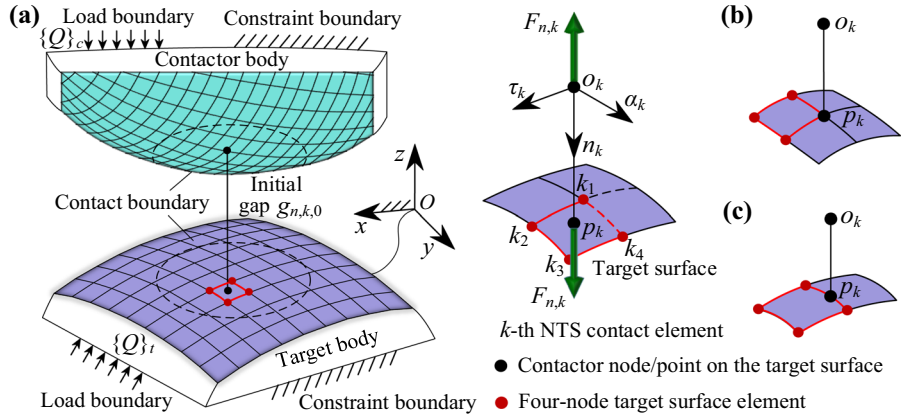

Fig. 1 Illustration of finite element contact problem and an NTS contact element configuration with point p_k being: **a** inside the target surface element; **b** at the node of surface element; **c** at the line of surface element

deviate from the initial direction. The effect is considered small and negligible in this paper. Otherwise, iterations or one time update may be employed to correct this deviation and improve the accuracy.

According to the assumptions, the initial gap $g_{n,k,0}$, the final contact gap $g_{n,k}$ and contact force $F_{n,k}$ are along the direction $\boldsymbol{n}_k$. Therefore, each NTS contact element, the contactor node and its potential surface element, is determined on the basis of the minimum distance between the contactor node and its paired potential contact surface.

For the k-th NTS contact element, the point p_k can lie inside the four-node target element, at any of the four nodes or on any of the four edges as illustrated in Fig. 1a, b and c. More than one contactor nodes are allowed to associate with a target surface element to form an effective NTS contact element. The required number of the NTS contact elements can be determined through a mesh sensitivity analysis to guarantee the accuracy of contact modeling.

The contact conditions, described by the following non-negative and complementarity conditions, are enforced to the NTS contact elements:

$$g_{n,k} \cdot F_{n,k} = 0,\ g_{n,k} \geq 0,\ F_{n,k} \geq 0,\ k = 1, 2, ..., m_c \tag{1}$$

where m_c is the number of contactor nodes.

In the finite element modeling of the node-to-surface linear complementarity problem (NTS-LCP), two component coordinate systems are attached to the contactor and target bodies respectively to establish component substructures. The component substructures are meshed with 8-node isoparametric elements and the structural stiffness is obtained in their own coordinate system. The target coordinate system is designated as the global coordinate system $\boldsymbol{S}\{O; x, y, z\}$. The structural stiffness of substructures can be transformed into global coordinate system by a standard finite element program [29]. For describing the gaps $g_{n,k}$ and forces $F_{n,k}$ of the NTS contact elements along contact direction $\boldsymbol{n}_k$ explicitly, the nodal coordinate system $\boldsymbol{S}_k\{o_k; n_k, \alpha_k, \tau_k\}$ is attached at the k-th potential contactor node o_k.

For the derivation of LCP equations, the gap-displacement and displacement-force functions are derived by geometric relationships and force equilibrium conditions in Sects. 2.2 and 2.3, respectively. Since the points p_k on the target surface elements are not consistent with the element nodes, a transformation between the nodal displacements/forces and the gap in the contact direction is needed. The final linear complementarity equations of the paired contact forces and gaps for all NTS contact elements are derived by eliminating the non-contact related nodal displacements and solved by a mathematical programming method effectively.

2.2 Gap-displacement relationships

Let the displacements $\{u_x, u_y, u_z\}_c$ of contactor nodes along the axes of global coordinate system $\{x, y, z\}$ form the nodal displacement vector $\{q\}_c$ as:

$$\{q\}_c = \left\{ \begin{matrix} \{u_x \quad u_y \quad u_z\}_{c,1} & \{u_x \quad u_y \quad u_z\}_{c,2} & \cdots \\ & \{u_x \quad u_y \quad u_z\}_{c,m_c} & \end{matrix} \right\}^{\mathrm{T}} \tag{2}$$

The displacements $\{u_n, u_\alpha, u_\tau\}_c$ of contactor nodes along the axes of nodal coordinate system $\{n_k, \alpha_k, \tau_k\}$ form the nodal displacement vector $\{q^*\}_c$ as:

$$\{q*\}_c = \left\{ \{u_n\}_c^{\mathrm{T}} \quad \{u_\alpha\}_c^{\mathrm{T}} \quad \{u_\tau\}_c^{\mathrm{T}} \right\}^{\mathrm{T}} \tag{3a}$$

where

$$\{u_J\}_c = \left\{u_{J,1}\, u_{J,2} \ldots u_{J,m_c}\right\}_c^{\mathrm{T}},\ J = n, \alpha, \tau \tag{3b}$$

The relationship between the displacements of the k-th contactor node along $\{x, y, z\}$ and $\{n_k, \alpha_k, \tau_k\}$ satisfies:

$$\begin{Bmatrix} u_x \\ u_y \\ u_z \end{Bmatrix}_{c,k} = \begin{bmatrix} \cos<x,n_k> & \cos<x,\alpha_k> & \cos<x,\tau_k> \\ \cos<y,n_k> & \cos<y,\alpha_k> & \cos<y,\tau_k> \\ \cos<z,n_k> & \cos<z,\alpha_k> & \cos<z,\tau_k> \end{bmatrix} \begin{Bmatrix} u_n \\ u_\alpha \\ u_\tau \end{Bmatrix}_{c,k} \tag{4}$$

where the operator $\cos<\ >$ is the cosine function of the angle between the two directions.

According to the Eqs. (2) and (4), the relationship between the displacement vectors of contactor nodes along $\{x, y, z\}$ and $\{n_k, \alpha_k, \tau_k\}$ satisfies:

$$\{q\}_c = [R]_c\{q*\}_c,\ [R]_c = [[R_n]\,[R_\alpha]\,[R_\tau]]_c \tag{5a}$$

$$[R_J]_c = \begin{bmatrix} \cos<x,J_1> & 0 & \cdots & 0 \\ \cos<y,J_1> & 0 & \cdots & 0 \\ \cos<z,J_1> & 0 & \cdots & 0 \\ 0 & \cos<x,J_2> & & \\ 0 & \cos<y,J_2> & \ddots & \\ 0 & \cos<z,J_2> & \ddots & \vdots \\ & 0 & \ddots & \\ \vdots & \vdots & & 0 \\ & & & \cos<x,J_{m_c}> \\ & & & \cos<y,J_{m_c}> \\ 0 & 0 & & \cos<z,J_{m_c}> \end{bmatrix},\quad J = n, \alpha, \tau \tag{5b}$$

where $[R]_c$ is the rotation transformation matrix from $\{n_k, \alpha_k, \tau_k\}$ to $\{x, y, z\}$.

Let the nodal displacement vectors of the target body and the k-th surface element along $\{x, y, z\}$ form the displacement vector $\{q\}_t$ and $\{q\}_{t,k}$ as:

$$\{q\}_t = \begin{Bmatrix} \{u_x \quad u_y \quad u_z\}_{t,1} & \{u_x \quad u_y \quad u_z\}_{t,2} & \cdots \\ & \{u_x \quad u_y \quad u_z\}_{t,m_t} & \end{Bmatrix}^{\mathrm{T}} \tag{6a}$$

$$\{q\}_{t,k} = \begin{Bmatrix} \{u_x \quad u_y \quad u_z\}_{t,k,1} & \{u_x \quad u_y \quad u_z\}_{t,k,2} \\ \{u_x \quad u_y \quad u_z\}_{t,k,3} & \{u_x \quad u_y \quad u_z\}_{t,k,4} \end{Bmatrix}^{\mathrm{T}} \tag{6b}$$

where m_t is the number of boundary nodes of target body.

The position of the displacement of the i-th node (i = 1,2,3,4) on the k-th target surface element in the displacement vector $\{q\}_t$ of the nodes on the target body can be expressed as:

$$\begin{Bmatrix} u_x \\ u_y \\ u_z \end{Bmatrix}_{t,k,i} = \begin{bmatrix} 0 & \cdots & 0 & 1 & 0 & \cdots & & & 0 \\ 0 & \cdots & & 0 & 1 & 0 & \cdots & & 0 \\ 0 & \cdots & & & 0 & 1 & 0 & \cdots & 0 \end{bmatrix}$$
$$\{q\}_t = [T]_{t,k,i}\{q\}_t,\ i = 1, 2, 3, 4 \tag{7}$$

From Eq. (7), the relationship between the displacements of the four nodes on the k-th surface element and the displacement vector $\{q\}_t$ can be expressed as:

$$\{q\}_{t,k} = [T]_{t,k}\{q\}_t,\ [T]_{t,k} = \begin{bmatrix} [T]_{t,k,1} \\ [T]_{t,k,2} \\ [T]_{t,k,3} \\ [T]_{t,k,4} \end{bmatrix} \tag{8}$$

where the nodal displacement vector of the k-th surface element $\{q\}_{t,k}$ is included in that of the target body $\{q\}_t$, and $[T]_{t,k}$ is the indicator matrix to describe the position of $\{q\}_{t,k}$ in $\{q\}_t$.

The displacement of point p_k can be determined by the nodal displacements of the k-th surface element by the shape function [29] as:

$$\begin{aligned} u^p_{J,t,k} &= [N(\zeta_k, \eta_k)]_k\{u_J\}_{t,k} \\ &= [N_{k,1}\, N_{k,2}\, N_{k,3}\, N_{k,4}]\{u_J\}_{t,k},\ J = x, y, z \end{aligned} \tag{9a}$$

$$\{u_J\}_{t,k} = \left\{u_{J,1}\, u_{J,2}\, u_{J,3}\, u_{J,4}\right\}_{t,k} \tag{9b}$$

where $[N]_k$ is the shape function, ζ_k and η_k are the local coordinate of p_k on the k-th surface element as shown in Fig. 2, $\{u_J\}_{t,k}$ are the elements of $\{q\}_{t,k}$ in Eq. (6b).

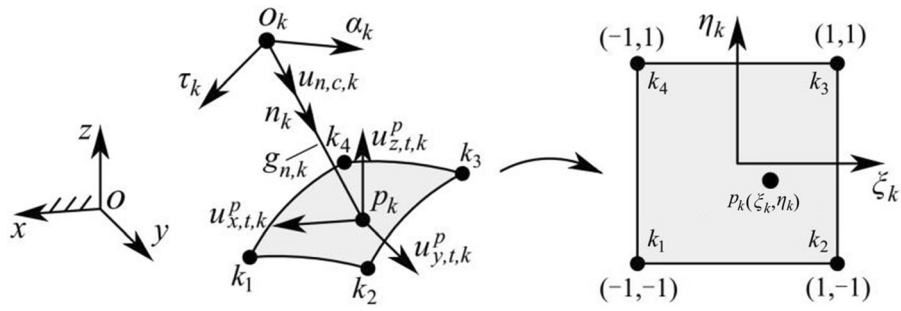

Fig. 2 Relationship between the contact gap and nodal displacements of the k-th NTS contact element after deformation

The other types of elements can be applied by modifying the number of nodes and shape function of surface elements in Eq. (6)-(9).

Projecting the displacements along the axes $\{x, y, z\}$ to the direction of $\boldsymbol{n}_k$, the gap-displacement relationships (between the contact gap and nodal displacements of the k-th NTS contact element after deformation shown in Fig. 2) can be expressed as:

$$\begin{aligned} g_{n,k} &= g_{n,k,0} + u^p_{x,t,k}\cos<x,n_k> + u^p_{y,t,k}\cos<y,n_k> \\ &\quad + u^p_{z,t,k}\cos<z,n_k> - u_{n,c,k} \\ &= g_{n,k,0} + [N(\xi_k,\eta_k)]\{u_x\}_{t,k}c_{k,1} \\ &\quad + [N(\xi_k,\eta_k)]\{u_y\}_{t,k}c_{k,2} \\ &\quad + [N(\xi_k,\eta_k)]\{u_z\}_{t,k}c_{k,3} - u_{n,c,k} \\ &= g_{k,0} + [R]_{t,k}\{q\}_{t,k} - u_{n,c,k} \end{aligned} \tag{10a}$$

$$\begin{aligned} [R]_{t,k} = \; & \left[N_{k,1}c_{k,1}N_{k,1}c_{k,2}N_{k,1}c_{k,3}N_{k,2}c_{k,1}N_{k,2}c_{k,2}\right. \\ & \left. N_{k,2}c_{k,3}\ldots N_{k,4}c_{k,1}N_{k,4}c_{k,2}N_{k,4}c_{k,3}\right] \end{aligned} \tag{10b}$$

where $c_{k,1} = \cos<x,n_k>$, $c_{k,2} = \cos<y,n_k>$, $c_{k,3} = \cos<z,n_k>$, $g_{n,k,0}$ is the initial contact gap, $u_{n,c,k}$ is the same as that of Eq. (4), $[R]_{t,k}$ is the rotation transformation matrix from the nodal displacements of the k-th surface element along the axes $\{x, y, z\}$ to the displacements of p_k along the contact direction.

The geometry function relationships between contact gaps and nodal displacements of all NTS contact elements can be derived by substituting Eqs. (3a, b), (5a, b) and (8) into Eq. (10a):

$$\begin{aligned} \{g_n\} &= \{g_{n,0}\} + [S]_t\{q\}_t - \{u_n\}_c,\ [S]_t \\ &= \begin{bmatrix} [R]_{t,1}[T]_{t,1} \\ [R]_{t,2}[T]_{t,2} \\ \cdots \\ [R]_{t,k}[T]_{t,k} \end{bmatrix},\ \{u_n\}_c = [\mathbf{1\,0\,0}][R]_c^{\mathrm{T}}\{q\}_c \end{aligned} \tag{11}$$

where $[R]_c^{\mathrm{T}}$ transforms the displacements of contactor nodes o_k along $\{x, y, z\}$ to that along contact directions $\boldsymbol{n}_k$, $[S]_t$ transforms the displacements of nodes on the target body along $\{x, y, z\}$ to that of points p_k along contact directions $\boldsymbol{n}_k$ through the indicator matrix $[T]_{t,k}$ in Eq. (8) and the rotation transformation matrix $[R]_{t,k}$ in Eq. (10b).

It can be seen that the gap-displacement relationships are explicitly described by the initial gap, the nodal displacements and the transformation matrix $[R]_c$ and $[S]_t$ between the nodal displacements $\{q\}_c$/$\{q\}_t$ along $\{x, y, z\}$ and displacements of o_k/p_k in the contact directions $\boldsymbol{n}_k$.

2.3 Equations of equilibrium for contactor and target bodies

For deriving the LCP equations of contact forces and gaps, the equilibrium equations of bodies' external contact forces/loads and internal deformation forces determined by nodal displacements and structural stiffness are established in this section.

Equilibrium equations of contactor body can be established based on the boundary nodes by employing the standard substructuring method [29] as:

$$[K]_c\{q\}_c = \{Q\}_c - \{Q_F\}_c,\ \{Q_F\}_c = [R]_c\begin{Bmatrix} \{F_n\} \\ \{F_\alpha\} \\ \{F_\tau\} \end{Bmatrix}_c \tag{12}$$

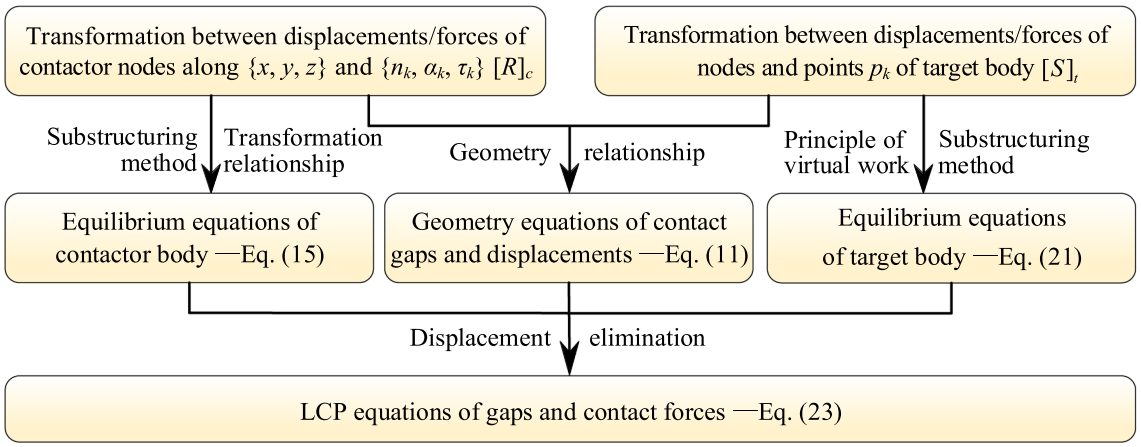

Fig. 3 The derivation process of the NTS scheme formulated into LCP

where $\{Q_F\}_c$ is composed of the contact forces projected along the direction of the axes $\{x, y, z\}$, $\{Q\}$ is the external load vector, $[K]$ is the structural stiffness matrix of the substructure in the global coordinate system.

Substituting the nodal displacement vectors of Eqs. (3a) and (5a) into Eq. (12) and left multiplying $[R]_c^{\mathrm{T}}$ which is the same as that in Eq. (11) transforming the forces of contactor nodes o_k along $\{x, y, z\}$ to that along $\{n_k, \alpha_k, \tau_k\}$, Eq. (12) becomes:

$$\begin{bmatrix} [K_{nn}] & [K_{n\alpha}] & [K_{n\tau}] \\ [K_{\alpha n}] & [K_{\alpha\alpha}] & [K_{\alpha\tau}] \\ [K_{\tau n}] & [K_{\tau\alpha}] & [K_{\tau\tau}] \end{bmatrix}_c \begin{Bmatrix} \{u_n\} \\ \{u_\alpha\} \\ \{u_\tau\} \end{Bmatrix}_c = \begin{Bmatrix} \{Q_n\} \\ \{Q_\alpha\} \\ \{Q_\tau\} \end{Bmatrix}_c - \begin{Bmatrix} \{F_n\} \\ \{F_\alpha\} \\ \{F_\tau\} \end{Bmatrix}_c \tag{13}$$

where $\begin{bmatrix} [K_{nn}] & [K_{n\alpha}] & [K_{n\tau}] \\ [K_{\alpha n}] & [K_{\alpha\alpha}] & [K_{\alpha\tau}] \\ [K_{\tau n}] & [K_{\tau\alpha}] & [K_{\tau\tau}] \end{bmatrix}_c = [R]_c^{\mathrm{T}}[K]_c[R]_c$,

$\begin{Bmatrix} \{Q_n\} \\ \{Q_\alpha\} \\ \{Q_\tau\} \end{Bmatrix}_c = [R]_c^{\mathrm{T}}\{Q\}_c$.

The contact related nodal displacements $\{u_n\}_c$ are the master degrees of freedom due to the friction forces are not considered in this paper, i.e. $\{F_\alpha\}_c = \mathbf{0}$, $\{F_\tau\}_c = \mathbf{0}$, and the Eq. (13) can be reconstructed as:

$$\begin{bmatrix} [K_{nn}] & [K_{n\beta}] \\ [K_{\beta n}] & [K_{\beta\beta}] \end{bmatrix}_c \begin{Bmatrix} \{u_n\} \\ \{u_\beta\} \end{Bmatrix}_c = \begin{Bmatrix} \{Q_n\} \\ \{Q_\beta\} \end{Bmatrix}_c - \begin{Bmatrix} \{F_n\} \\ \mathbf{0} \end{Bmatrix}_c \tag{14}$$

Eliminating the nodal displacements $\{u_\beta\}_c$ along the two tangential directions $\boldsymbol{\alpha}$ and $\boldsymbol{\tau}$, the equilibrium equations of contactor body along the contact directions $\boldsymbol{n}$ are written as:

$$[\overline{K}_{nn}]_c\{u_n\}_c = \{\overline{Q}_n\} - \{F_n\} \tag{15}$$

where $[\overline{K}_{nn}]_c = [K_{nn}]_c - [K_{n\beta}]_c[K_{\beta\beta}]_c^{-1}[K_{\beta n}]_c$, $\{\overline{Q}_n\}_c = \{Q_n\}_c - [K_{n\beta}]_c[K_{\beta\beta}]_c^{-1}\{Q_\beta\}_c$.

Equilibrium equations of target body, likewise, are established based on the boundary nodes as:

$$[K]_t\{q\}_t = \{Q\}_t + \{Q_F\}_t \tag{16}$$

where $\{Q_F\}_t$ is composed of the nodal contact forces along the axes $\{x, y, z\}$ which is equivalent to the contact forces of points p_k along contact directions.

The point p_k is usually not consistent with the nodes of meshes on the target body. According to the principle of virtual work, the virtual work done by the non-nodal forces along the virtual displacements is equal to that of the equivalent nodal forces, so that the contact forces of the points p_k (non-nodal forces) can be transformed to the nodal forces of target body $\{Q_F\}_t$. The virtual displacements of points p_k and nodes of target body are $\{\delta u^p_{x,t,k}, \delta u^p_{y,t,k}, \delta u^p_{z,t,k}\}$ and $\delta\{q\}_t$ respectively, both along the axes of global coordinate system $\{x, y, z\}$.

The virtual work of the contact force $F_{n,k}$ along the virtual displacements of p_k is:

$$\begin{aligned}\delta W_{t,k} &= F_{n,k}\cos<x,n_k>\delta u^p_{x,t,k} + F_{n,k}\cos<y,n_k\\ &>\delta u^p_{y,t,k} + F_{n,k}\cos<z,n_k>\delta u^p_{z,t,k}\\ &= F_{n,k}[R]_{t,k}\delta\{q\}_{t,k} = F_{n,k}[R]_{t,k}[T]_{t,k}\delta\{q\}_t\end{aligned} \tag{17}$$

where $[R]_{t,k}$ is the transformation matrix which is the same as that in Eq. (10b).

According to Eqs. (11) and (17), the virtual work of all potential contact forces along the virtual displacements of p_k is:

$$\begin{aligned}\delta W_t &= \sum_{k=1}^{m_c}\delta W_{t,k} = \sum_{k=1}^{m_c} F_{n,k}[R]_{t,k}[T]_{t,k}\delta\{q\}_t\\ &= \{F_n\}^{\mathrm{T}}[S]_t\delta\{q\}_t\end{aligned} \tag{18}$$

where $[S]_t$ transforms the virtual displacements of nodes $\delta\{q\}_t$ along $\{x, y, z\}$ to that of points p_k along contact directions $\boldsymbol{n}_k$, the same as that in Eq. (11).

The virtual work of all nodal forces of target body along the virtual displacements $\delta\{q\}_t$ can be expressed as:

$$\delta W_t = \{Q_F\}_t^{\mathrm{T}}\delta\{q\}_t \tag{19}$$

According to the principle of virtual work, Eqs. (18) and (19), the contact forces of points p_k can be transformed to the nodal forces as:

$$\{Q_F\}_t = [S]_t^{\mathrm{T}}\{F_n\} \tag{20}$$

where $[S]_t$ transforms the forces of nodes on the target body along $\{x, y, z\}$ to that of points p_k along contact directions $\boldsymbol{n}_k$, which is derived by the principle of virtual work.

Substituting the Eq. (20) into Eq. (16), the equilibrium equations of target body are expressed as:

$$[K]_t\{q\}_t = \{Q\}_t + [S]_t^{\mathrm{T}}\{F_n\} \tag{21}$$

It can be seen from Eqs. (13) and (21) that displacement-force functions derived by the force equilibrium conditions are described by substructure stiffness, nodal displacements, external loads, contact forces, and the transformation $[R]_c$ and $[S]_t$ between the nodal forces $\{Q_F\}_c/\{Q_F\}_t$ along $\{x, y, z\}$ and forces of o_k/p_k in the contact directions. Combined the equilibrium equations with the gap-displacement relationships to eliminate the displacement vectors, the specific expression of the LCP equations can be derived in Sect. 2.4.

2.4 Formulation of LCP

The derivation strategy for formulating the NTS-LCP scheme is schematically shown in Fig. 3. The equilibrium equations, Eqs. (15) and (21), in a partitioned form, are substituted into the geometry equations Eq. (11) to eliminate the nodal displacements, and the relationships of contact gaps and forces are derived as:

$$\begin{aligned}\{g_n\} = \{g_{n,0}\} &+ [S]_t[K]_t^{-1}\left(\{Q\}_t + [S]_t^{\mathrm{T}}\{F_n\}\right)\\ &- [\overline{K}_{nn}]_c^{-1}\left(\{\overline{Q}_n\} - \{F_n\}\right)\end{aligned} \tag{22}$$

Thus, the LCP equations can be derived as:

$$\begin{cases}\{F_n\} - [M_n^*]\{g\} = \{Q_n^*\}\\ [M_n^*] = [A]^{-1}[\overline{K}_{nn}]_c,\ \{Q_n^*\} = [A]^{-1}(\{\overline{Q}_n\}\\ -[\overline{K}_{nn}]_c\{g_{n,0}\} - [\overline{K}_{nn}]_c[S]_t[K]_t^{-1}(\{Q\}_t))\\ \{F_n\}\cdot\{g_n\} = \mathbf{0},\ \{F_n\}\geq 0,\ \{g_n\}\geq 0\end{cases} \tag{23}$$

where $[A] = [\overline{K}_{nn}]_c[S]_t[K]_t^{-1}[S]_t^{\mathrm{T}} + [I]$, $[I]$ is the identity matrix.

3 Finite element modeling and NTS-LCP formulation

3.1 General description of proposed contact approach

In the LCP equations, the main factors are of the initial contact gaps, structural stiffness, and the transformation matrix. The general contact approach based on the NTS-LCP scheme, for finite element modeling and NTS-LCP formulation, is summarized as the flow chart shown in Fig. 4, and the detailed steps are explained as follows:

(1) Given the geometry and physical parameters of two elastic bodies, manufacturing and assembly errors, and boundary conditions of constraints and loads.
(2) Build the geometry model, generate meshes of two elastic bodies under ideal condition, and specify the contactor and target bodies.
(3) Select the boundary nodes of two bodies, set the global coordinate system on the target body, and

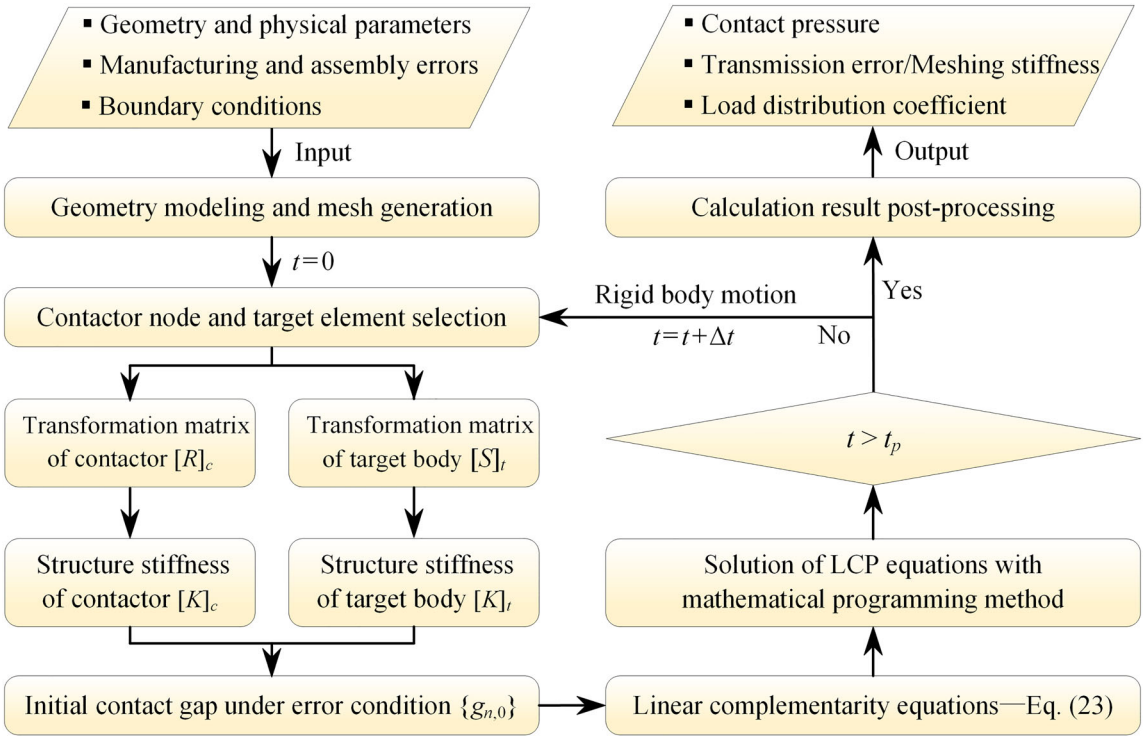

Fig. 4 The flow chart of the general contact approach based on the NTS-LCP scheme

obtain the coordinates of nodes for determining the initial contact gaps, normal contact direction and shape function of p_k; set the nodal coordinate systems at the boundary nodes of contactor body to calculate the transformation matrix $[R]_c$ by using Eq. (5); obtain the shape function $[N]_k$ of p_k and the indicator matrix $[T]_k$ of the k-th surface element by using Eqs. (7)-(8), and obtain the transformation matrix $[S]_t$ by Eq. (11).

(4) Obtain the structural stiffness by substructuring method and impose boundary conditions.
(5) Calculate the initial gaps $\{g_{n,0}\}$ under error condition.
(6) Construct the LCP equations by Eq. (23) and employ the mathematical programming method (e.g. Lemke method) to solve the complementarity equations. The detailed iterative solution of LCP equations is presented in Ref. [30].
(7) Apply the rigid body motion to the contactor and target body, update the contact boundary at this time/position, and repeat steps 3 to 6 until the time is greater than the specified time t_p.
(8) Post-process and output the calculation results, such as contact pressure, load distribution, transmission error, etc.

3.2 Application to contact between deformable gears

In this section, the NTS-LCP scheme described in the previous section is adapted to handling contact between two gears. The procedure is described below.

(1) Given the geometry parameters of pinion and wheel, manufacturing and assembly errors, and boundary conditions of constraints and torque.
(2) Establish the geometry model of each gear according to the generating principle of gear yielded by rack and generate the mesh employing the node connection approach [31, 32]. The pinion is referred as the target body and the wheel as the contactor body.
(3) Select the nodes on the contact boundary of wheel in the potential contact region near the contact line determined by meshing theory, and

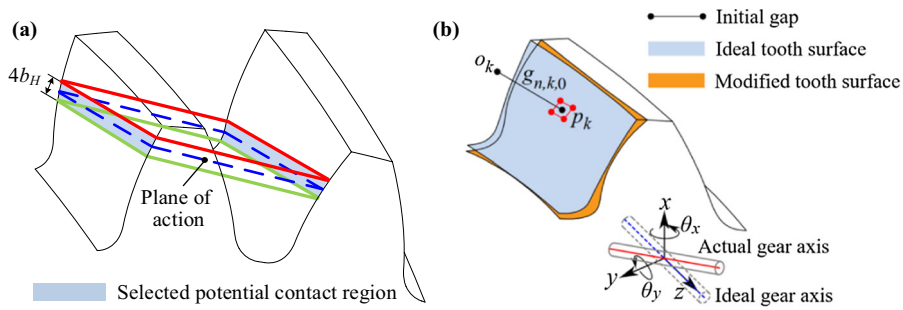

Fig. 5 Potential contact region and initial contact gaps at an instant: **a** potential contact region; **b** initial contact gaps with errors

specify the width of the potential contact region to be four times of Hertz contact half width b_H [1, 31, 32] shown in Fig. 5(a); determine the contact direction of each contactor node and its potential target surface element according to Sect. 2.1; couple the nodes of the gear holes to their central nodes for imposing the load and constraint boundary conditions; establish the global coordinate system at the central node of pinion and the nodal coordinate system at the boundary nodes of wheel to obtain the coordinates of boundary nodes, transformation matrix, shape function and indicator matrix as the step 3 in Sect. 3.1.

(4) Obtain the structural stiffness matrixes of pinion and wheel by using substructuring method; fix the central node of wheel fully, and that of pinion except the rotational degree of freedom; impose the constraint boundary conditions by means of penalty approach [29].

(5) Obtain the coordinates of contactor nodes and target surface element nodes in the global coordinate system under error condition [25, 33, 34] as shown in Fig. 5(b), and determine the initial contact gaps $o_k p_k$.

(6) Construct the LCP equations by Eq. (23), and employ the Lemke method to solve the equations to obtain the contact force of each NTS contact element.

(7) Divide the angle corresponding to one meshing period t_p into n equal parts, and the rotation angles $\Delta\varphi_1$ and $\Delta\varphi_2$ of pinion and wheel for each calculation are:

$$t_p = \frac{p_n}{r_{b1}},\ \Delta\varphi_1 = \frac{t_p}{n},\ \Delta\varphi_2 = \frac{t_p}{n}\frac{z_1}{z_2} \tag{24}$$

where p_n is the normal pitch, r_{b1} is the radius of base circle of pinion, z_1 and z_2 are the tooth number of pinion and wheel respectively. Repeat the steps 3 to 6 after gear rotation until the time is greater than the specified time t_p.

(8) Post-process and output the results by the calculated contact forces, including contact pressure, load distribution and meshing stiffness as shown in Fig. 6:

(a) The contact pressure of each node can be obtained by the ratio of contact force and corresponding area of the node [17]. For example, the competence area of the k-th node is the average area of its adjacent elements (S_1, S_2, S_3, S_4).

(b) The load distribution can be obtained by the slice method. The gear tooth is divided into m slices along the direction of tooth face width, and the load distribution of per unit width b_{ij} is calculated by the ratio of the sum of the contact forces of all nodes in the i-th slice and the width of the slice, as shown in Fig. 6, where $i = 1,2,\ldots,m$, and j is the number of engaged gear teeth. The load distribution coefficient K_H [35–37] is the index to measure the uniformity of load distribution along the tooth face width direction which is calculated as:

$$K_H = \max_{i,\varphi} \sum_j b_{ij}(\varphi) \Big/ \operatorname*{mean}_{i,\varphi} \sum_j b_{ij}(\varphi) \tag{25}$$

where max and mean is the maximum and mean operator.

(c) The transmission error TE can be determined by substituting the contact forces into Eq. (15) and

calculating the rotation angle of the central node. The meshing stiffness can be obtained by transmission error TE and torque T as:

$$K_m = \frac{T}{(r_{b2}\cos\beta_b)^2 TE} \tag{26}$$

where r_{b2} is the radius of base circle of wheel, β_b is the helix angle of base circle.

The NTS-LCP scheme based contact approach is implemented into a computer code written in Matlab language and the numerical results are performed in Sect. 4.

4 Example applications

The contact of a cam and a follower, and gear pairs are simulated by means of the Hertz method, ANSYS and the proposed NTS-LCP scheme. The contact characteristics including contact pressure, load distribution and meshing stiffness of spur and helical gear pairs with tooth modifications and assembly error are further analyzed by using the proposed NTS-LCP scheme.

4.1 Contact analysis of a cam and a follower

The schematic diagram and finite element contact model of a cam-follower is shown in Fig. 7 of which the geometry and physical parameters are listed in Table 1. The motion of the roller follower satisfies the harmonic function: $h(1\text{-}\cos\varphi)/2$, where, h is the amplitude of motion and φ is the rotation angle of cam. The cam and follower are meshed using the refined linear tetrahedron elements in the contact region and linear hexahedral elements in the other region. The load and constraint boundary conditions are imposed on the central nodes of cam and follower as shown in Fig. 7b. To ensure the convergence of the numerical solutions, the mesh sensitivity analysis is conducted for the ANSYS model and the proposed NTS-LCP scheme. The maximum contact pressures are plotted against the number of nodes N_1 and N_2 along the width direction and length direction in the contact region in Fig. 8. It can be seen that the NTS-LCP scheme converges more rapidly than ANSYS. The two sets of results are also in good agreement. The proposed scheme and ANSYS model converge if $N_1 = 11$ and $N_2 = 20$ are used in the component meshing. This yields a total number of finite element nodes of 418 335.

With the Hertz contact method, ANSYS and NTS-LCP scheme, the contact pressure distribution along the contact width at the initial position ($\varphi = 0$) is obtained and shown in Fig. 9. The maximum contact pressure P_m with the three methods is 689 MPa, 684 MPa and 687 MPa, respectively. The maximum difference is only 0.7%. The computing time with the

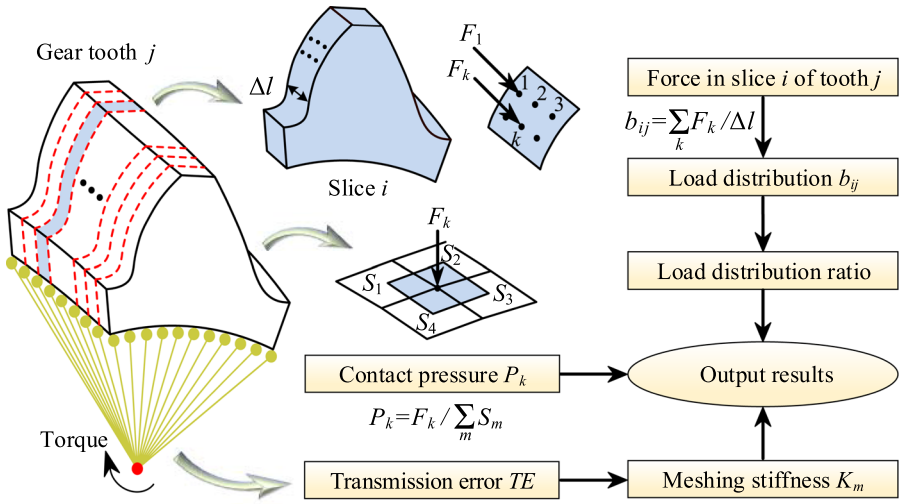

Fig. 6 Post-process to obtain the contact characteristics of gear pairs including contact pressure, load distribution and meshing stiffness

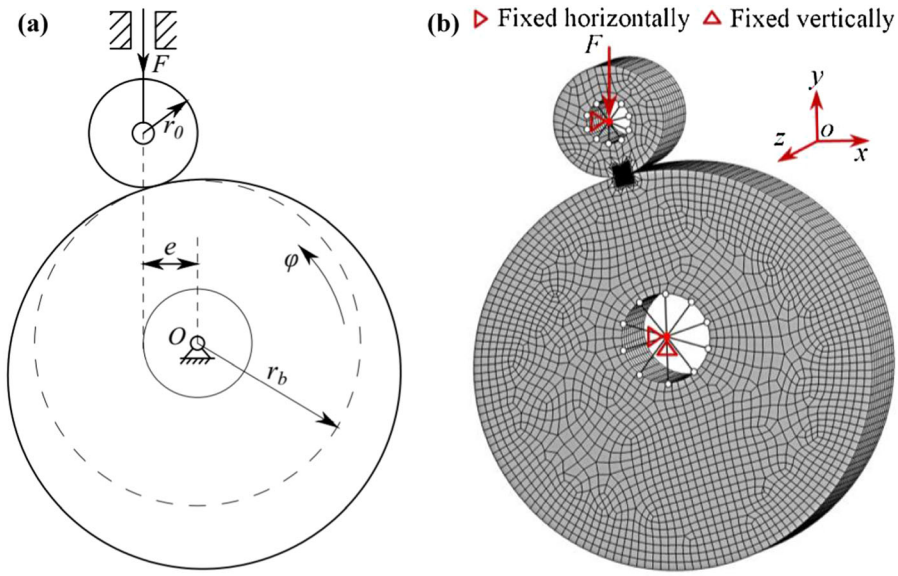

Fig. 7 Contact of a cam and a follower: **a** schematic diagram of a cam-follower; **b** finite element contact model of cam-follower

Table 1 Geometry and physical parameters of the cam-follower

Parameters	Values (mm)	Parameters	Values
Radius of cam base circle r_b	20	Amplitude of motion h	6 mm
Radius of roller follower r_0	5	Elastic modulus	206GPa
Eccentricity e	5	Poisson ratio	0.3
Width of cam and roller	10	Vertical load F	500 N

ANSYS and NTS-LCP scheme on a CPU E5-2667 server is 1275 s and 310 s, respectively. There is good agreement among the three sets of results obtained using three different methods. The proposed NTS-LCP scheme is computationally more efficient than ANSYS.

4.2 Contact analysis of spur and helical gear pairs

The contact between a pair of spur gears and helical gears is analyzed by the proposed NTS-LCP scheme according to the procedure described in Sect. 3.2. The geometry and physical parameters of the spur and helical involute gear pairs are given in Table. 2. The hypothetical manufacturing and assembly errors considered in this case involve the tooth profile modification, the lead modification and the misalignment error of gear axis. The tooth profile modification consists of the tip relief and lead crown modification. The tip relief is described by the length of profile modification L_a and the amount of profile modification C_a [38, 39] while lead crown modification can be described by lead crowning amount C_l [32, 39, 40]. For the convenience of discussion, the tooth modifications adopt linear tip relief and parabolic lead crown relief [38], and the misalignment error is parallel to the plane of action in this section.

Both spur and helical gear sets are meshed using the linear hexahedral elements. The finite element meshes and boundary conditions in the contact regions are shown in Fig. 10. At the initial position, the first pair of spur gear teeth engages at the pitch circle while that of the helical gear tooth in the rear transverse engages at the pitch circle. The second/third pair of spur/helical gear teeth tends to engage. The applied torque T is 300 Nm. The mesh sensitivity analysis with a misalignment error $\varepsilon = 10$ μm is conducted by ANSYS and the NTS-LCP scheme. The numerical results are shown in

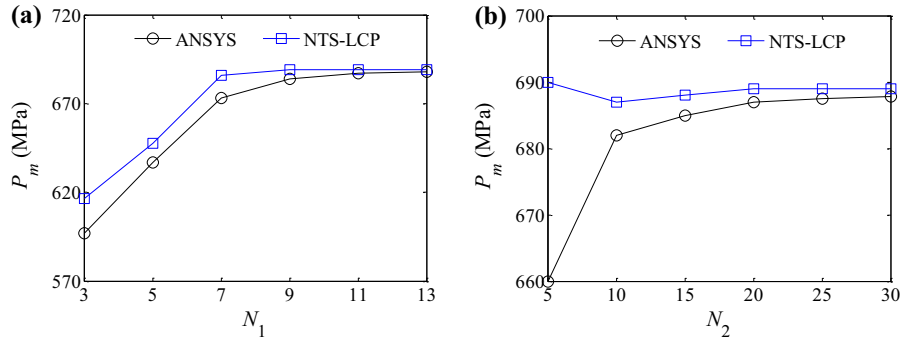

Fig. 8 Mesh sensitivity analysis of cam-follower contact problem: **a** sensitivity analysis along contact width direction; **b** sensitivity analysis along contact length direction

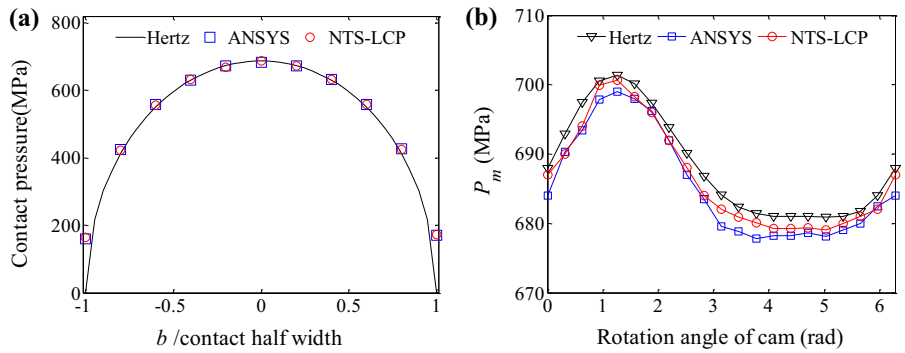

Fig. 9 Contact pressure of the cam-follower: **a** contact pressure distribution along contact width direction at the initial position ($\varphi = 0$); **b** maximum contact pressure with cam rotation

Fig. 11. It can be seen that the proposed scheme yields a nicely converged solution, and $N_1 = 11$ and $N_2 = 60$ are used in the finite element meshing. The number of nodes of spur and helical gear pairs is 649 775 and 1 087 261 respectively. The results of the maximum contact pressure P_m and the computational time for a complete gear contact analysis under the ideal condition obtained by ANSYS and the NTS-LCP scheme are given in Tables 3 and 4. It can be concluded that the accuracy and efficiency of the proposed NTS-LCP scheme are valid for the gear contact analysis. Table. 4 shows that the computational time spent in finding the structural stiffness takes about 90% of the total time. For contact analysis with different cases of geometric errors, the computational time associated with the NTS-LCP scheme itself is only 10% because of the restructuring. It can be concluded that the proposed scheme is advantageous in dealing with contact because of the significantly reduced problem size, suited for investigating effects of errors on contact characteristics.

The transmission errors of the spur gear pair with different tooth profile modifications, expressed in terms of linear displacement along the line of action, are shown in Fig. 12. The length of profile modification L_a taken in the case study is less than the distance from the tooth tip to the highest point of single tooth contact on the involute profile [41], which is 2.52 mm for the spur gear pair in Table. 2. Figure 12a shows that the gear transmission error of double-tooth contact region increases with the modification amount C_a; the peak-to-peak transmission error with gear rotation is reduced from 4.3 μm to 0.5 μm, which is beneficial to the dynamic behaviors of gear contact

Table 2 Geometry and physical parameters of spur and helical involute gear pairs

Parameters	Spur gear	Helical gear	Parameters	Spur gear	Helical gear
Gear tooth z_1/z_2	36/36	36/36	Helix angle β_b	0	15°/-15°
Normal modulus	3 mm	3 mm	Elastic modulus	2.06GPa	2.06GPa
Pressure angle	20°	20°	Poisson ratio	0.3	0.3
Transversal/face contact ratio	1.692/0	1.613/0.824	Addendum/dedendum coefficient	1/1.25	1/1.25
Gear width	30 mm	30 mm			

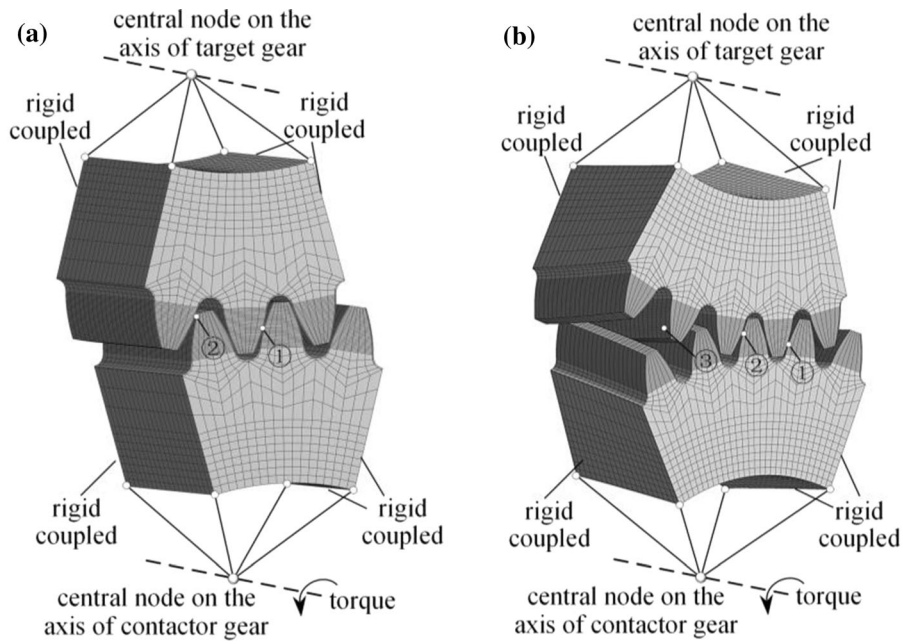

Fig. 10 Finite element contact analysis of gear pairs: **a** spur gear pair; **b** helical gear pair

[27, 38]. The peak-to-peak transmission errors with different torques, L_a and C_a are shown in Fig. 12b and c. The reduction of the peak-to-peak transmission error is not obvious for small modification lengths L_a = 0.5, 1.0, and 1.5 mm. Moreover, the profile modification amount should be appropriate and the optimal amounts vary with torques. For pledging the robustness of the modification effects within the interested ranges of operating torque [42, 43], e.g. 200Nm to 400 Nm, the peak-to-peak transmission errors for different torques T and amount of profile modifications C_a are shown in Fig. 12d. The maximum peak-to-peak transmission error for T = 200-400Nm and C_a = 5/7.5/10/12.5/15 μm is 3.3/2.3/1.7/2.8/4.0 μm, respectively. The modification amount C_a = 10 μm is proper for this case. With the help of parametric study by means of the proposed contact scheme, the proper modification amount can be efficiently determined.

The maximum contact pressure of the helical gear pair along the face width at the initial position is shown in Fig. 13. It can be seen from Fig. 13a that the stress concentration exists at the starting and leaving contact position. The tooth profile modification reduces the maximum contact pressure from 1512 to 772 MPa as shown in Fig. 13b. Figure 14 shows the load distribution of the helical gear pair with misalignment error and lead modification. With lead

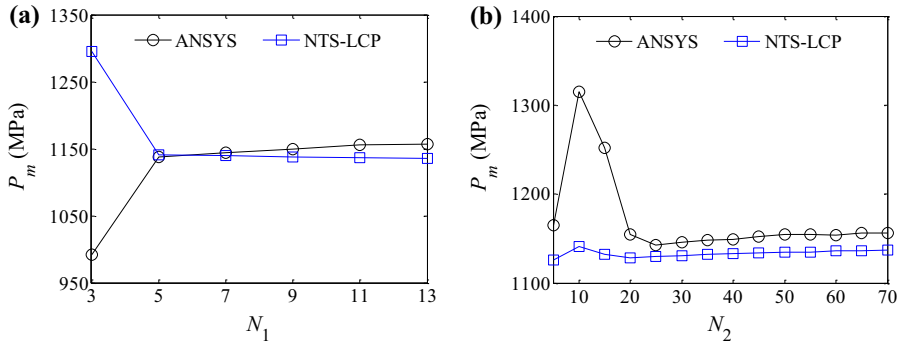

Fig. 11 Mesh sensitivity analysis of spur gear contact problem with misalignment error $\varepsilon = 10$ μm: **a** sensitivity analysis along contact width direction; **b** sensitivity analysis along contact length direction

Table 3 Maximum contact pressure of gears at the initial position under ideal condition

Items	Hertz (MPa)	ANSYS (MPa)	NTS-LCP (MPa)	Difference (%)
Spur gear pair contact	877	934	922	1.3
Helical gear pair contact	–	1473	1512	2.6

Table 4 Computing time of ANSYS and NTS-LCP scheme

	Items	Cam-follower	Spur gears	Helical gears
Ansys	Total time of ANSYS	1275 s	2620 s	7860 s
NTS-LCP	Structural stiffness obtained	290 s	500 s	1220 s
	LCP equations solved	20 s	35 s	100 s
	Total time of NTS-LCP	310 s	535 s	1320 s
	Time of ANSYS/Time of NTS-LCP	4.11	4.90	5.95

modification, the maximum load tends to distribute towards the middle of face width and the load distribution coefficient decreases from 2.11 to 1.68. It can be concluded from Fig. 13 and Fig. 14 that the tooth profile modification can alleviate stress concentrations and lead modification can improve the uniformity of load distribution.

For further analyzing the effects of tooth modifications on gear contact characteristics, the maximum contact pressure and load distribution coefficients with different modifications are simulated as shown in Fig. 15. Figure 15a shows the maximum contact pressure P_m with different profile modification amount C_a and length L_a. With the increase of profile modification amount C_a, the maximum contact pressure first decreases and then increases, and the optimum amount is larger with the longer modification length. If the modification length is short, e.g. $L_a = 0.5$ mm, the maximum contact pressure increases sharply with the increase of modification amount, and if the modification length is too long, e.g. $L_a = 1.5$ mm, the maximum contact pressure is always larger than that with $L_a = 1$ mm. Therefore, the proper profile modification length and amount are $L_a = 1$ mm and $C_a = 3$ μm.

The load distribution coefficients with $L_a = 1$ mm, $C_a = 3$ μm, and different lead modification amount C_l are shown in Fig. 15b. The load distribution coefficient with $C_l = 5$ μm is smaller than that with $C_l = 0$ μm as $|\varepsilon| \geq 5$ μm, while it is smaller than that with $C_l = 10$ μm as $|\varepsilon| \leq 20$ μm, which indicates that the lead modification $C_l = 5$ μm is preferable for the load distribution uniformity. It can be concluded that lead modification can improve the uniformity of load

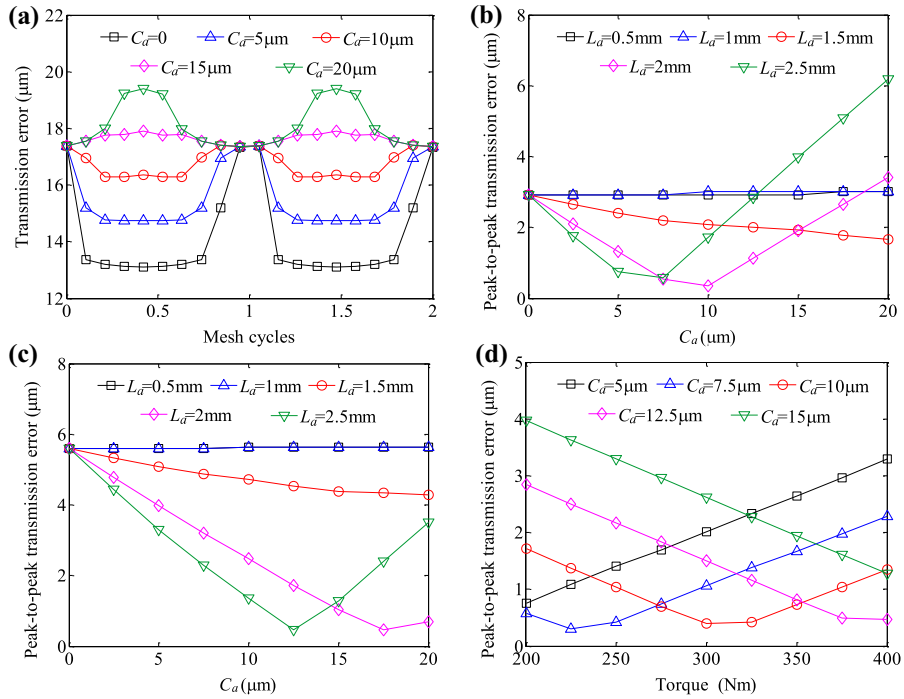

Fig. 12 Transmission errors of the spur gear pair with different profile modifications and torques: **a** transmission error with T = 300Nm, L_a = 2 mm and different C_a; **b/c** peak-to-peak transmission error with T = 200/400Nm, different L_a and C_a; **d** peak-to-peak transmission error with L_a = 2.5 mm, different T and C_a

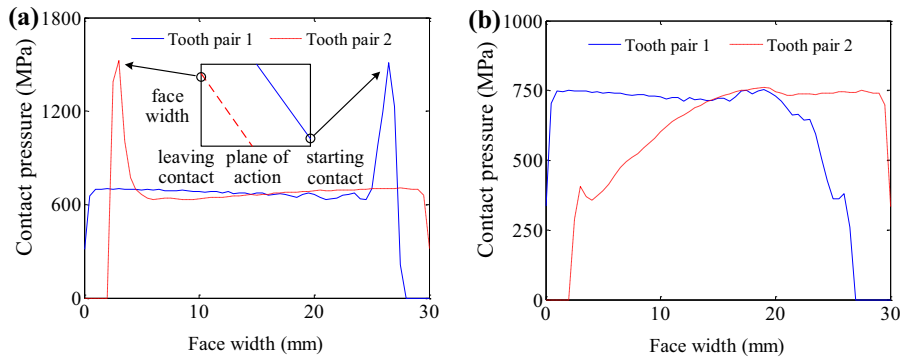

Fig. 13 Contact pressure on the line of contact for the helical gear pair at the initial position with T = 300Nm and: **a** without tooth modification; **b** with tooth profile modification amount C_a = 4 μm and modification length L_a = 1 mm

distribution, and the proper modification amount can be determined by the simulation based on the NTS-LCP scheme.

The gear meshing stiffness of the helical gear pair with T = 300Nm, ε = 0/5/10 μm and lead modification is shown in Fig. 16. It can be seen that the misalignment error greatly reduces the meshing stiffness as shown in Fig. 16a and the tooth lead modification can reduce the effect of misalignment error on the meshing stiffness shown in Fig. 16b.

The contact behaviors of cam-follower and gear pairs are successfully simulated by the proposed NTS-

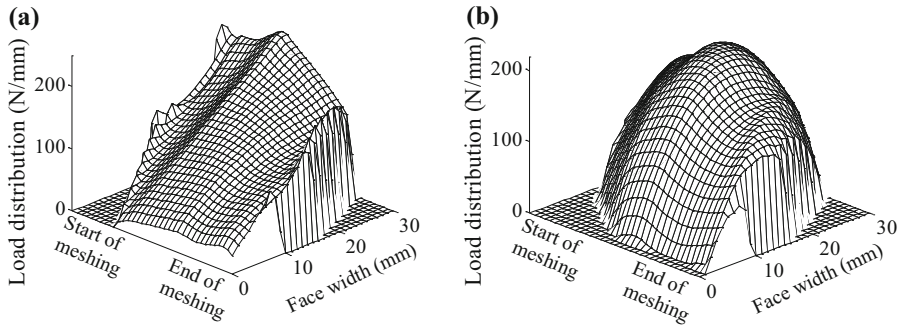

Fig. 14 Load distribution of the helical gear pair with T = 300Nm and: **a** with misalignment error ε = 10 μm; **b** with misalignment error ε = 10 μm and lead modification C_l = 5 μm

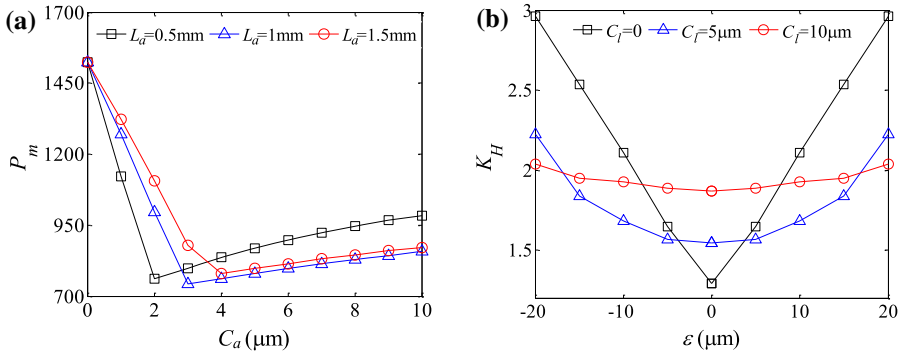

Fig. 15 Maximum contact pressure and load distribution coefficients with T = 300Nm and tooth modifications: **a** maximum contact pressure; **b** load distribution coefficients with L_a = 1 mm and C_a = 3 μm

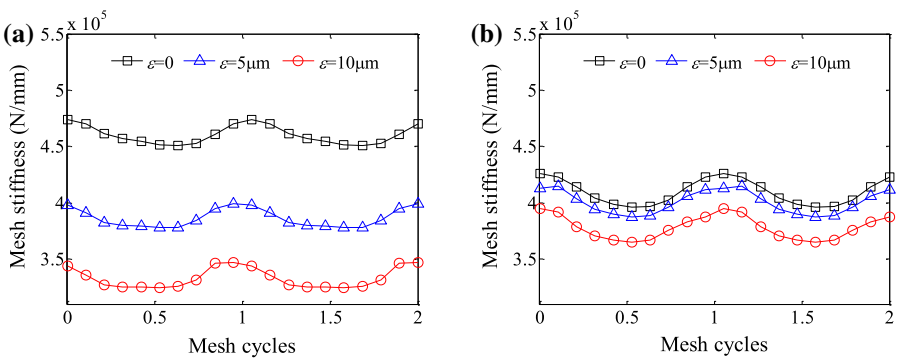

Fig. 16 Meshing stiffness of the helical gear pair with T = 300Nm, misalignment error ε = 0/5/10 μm and: **a** without modification; **b** with C_l = 5 μm

LCP scheme. The correct predictions of the effects of torque, tooth profile modification, lead modification and misalignment error on contact pressure, load distribution and gear meshing stiffness show the versatility and significance of the proposed approach.

5 Conclusions

An effective and original NTS-LCP scheme, valid for conforming and non-conforming meshes without the need for re-meshing, is presented in this paper to simulate general contact between three-dimensional deformable bodies. Using the proposed scheme, a nonlinear contact problem is transformed into a linear complementarity problem for which a reliable solution

can be found with the mathematical programming method. The numerical results obtained using the proposed scheme were compared with those of ANSYS and the Hertz contact formulas for cam-follower contact and gears contact. Good agreement was observed. The proposed scheme possesses the consistent computational accuracy and higher efficiency compared to the ANSYS benchmark solution.

The effects of tooth modifications on contact characteristics of spur gears and helical gears were investigated with the proposed scheme. The examples indicate that the proposed NTS-LCP scheme is versatile for investigating the contact characteristics, which involves the contact pressure, load distribution and meshing stiffness, of three-dimensional contact between gears with geometric errors. The proper tooth modifications obtained from the scheme can improve the uneven load distribution caused by the misalignment error, reduce peek-to-peek transmission error of spur gears and alleviate stress concentrations of helical gear pairs. The work reported in this paper provides a new and efficient approach for assessing contact-related performance of mechanical systems.

Funding This work was supported by the National Key R&D Program of China (No. 2018YFB2001504) and the National Natural Science Foundation of China (No. 52175045, No. U1808213).

Declarations

Conflict of interest All the authors declare that they have no conflicts of interest.

References

1. Hertz H (1881) On the contact of elastic solids. J Reine Agnew Math 92:156–171
2. Hu Y, Talbot D, Kahraman A (2018) A load distribution model for planetary gear sets. J Mech Des 140(5):053302
3. Feng M, Ma H, Li Z, Wang Q, Wen B (2018) An improved analytical method for calculating time-varying mesh stiffness of helical gears. Meccanica 53(4):1131–1145
4. Cappellini N, Tamarozzi T, Blockmans B, Fiszer J, Cosco F, Desmet W (2018) Semi-analytic contact technique in a non-linear parametric model order reduction method for gear simulations. Meccanica 53(1):49–75
5. Gonzalez-Perez I, Fuentes-Aznar A (2018) Implementation of a finite element model for gear stress analysis based on tie-surface constraints and its validation through the Hertz's theory. J Mech Des 140(2):023301
6. Parker R, Agashe V, Vijayakar S (2000) Dynamic response of a planetary gear system using a finite element/contact mechanics model. J Mech Des 122(3):304–310
7. DeMul JM, Vree JM, Maas DA (1989) Equilibrium and associated load distribution in ball and roller bearings loaded in five degrees of freedom while neglecting friction-Part I: general theory and application to ball bearings. J Tribol 111(1):142–148
8. Yu S, Wang D, Dong H, Wang B (2013) A new method for determining load distributions among rollers of bearing with manufacturing errors. Proc Inst Mech Eng Part C-J Eng Mech Eng Sci 227(11):2402–2415
9. Fiszer J, Tamarozzi T, Desmet W (2016) A semi-analytic strategy for the system-level modelling of flexibly supported ball bearings. Meccanica 51(6):1503–1532
10. Koshy CS, Flores P, Lankarani HM (2013) Study of the effect of contact force model on the dynamic response of mechanical systems with dry clearance joints: Computational and experimental approaches. Nonlinear Dyn 73:325–338
11. Kanto Y, Yagawa G (1990) A dynamic contact buckling analysis by the penalty finite element method. Int J Numer Methods Eng 29:755–774
12. Zmitrowicz A (2010) Contact stresses: A short survey of models and methods of computations. Arch Appl Mech 80:1407–1428
13. Billups SC, Murty KG (2000) Complementarity problems. J Comput Appl Math 124:303–318
14. Meingast M, Legrand M, Pierre C (2014) A linear complementarity problem formulation for periodic solutions to unilateral contact problems. Int J Non-Linear Mech 66:18–27
15. Jin S, Sohn D, Im S (2016) Node-to-node scheme for three-dimensional contact mechanics using polyhedral type variable-node elements. Comput Methods Appl Mech Engrg 304:217–242
16. Kim J, Lim J, Lee J, Im S (2008) A new computational approach to contact mechanics using variable-node finite elements. Int J Numer Methods Engrg 73(13):1966–1988
17. Wautelet G, Papeleux L, Ponthot JP (2016) The influence of equivalent contact area computation in 3D extended node to surface contact elements. Key Eng Mater 68:19–46
18. Zavarise G, Lorenzis L (2009) A modified node-to-segment algorithm passing the contact patch test. Int J Numer Meth Engng 79:379–416
19. Khoei A, Biabanaki S, Parvaneh S (2013) 3D dynamic modeling of powder forming processes via a simple and efficient node-to-surface contact algorithm. Appl Math Model 37:443–462
20. Gonzalez-Yuste J, Montenegro R, Escobar J, Montero G, Rodriguez E (2004) Local refinement of 3-D triangulations using object-oriented methods. Adv Eng Softw 35:693–702
21. Staten M, Shepherd J, Ledoux F, Shimada K (2010) Hexahedral mesh matching: converting non-conforming hexahedral-to-hexahedral interfaces into conforming interfaces. Internat J Numer Methods Engrg 82:1475–1509
22. Xing W, Zhang J, Song C, Tin-Loi F (2019) A node-to-node scheme for three-dimensional contact problems using the scaled boundary finite element method. Comput Methods Appl Mech Eng 347:928–956

23. Conry TF, Seireg A (1971) A mathematical programming method for design of elastic bodies in contact. J Appl Mech 38(2):387–392
24. Conry TF, Seireg A (1973) A mathematical programming technique for the evaluation of load distribution and optimal modifications for gear systems. J Eng Ind-Trans ASME 95(4):1115–1122
25. Li S (2007) Finite element analyses for contact strength and bending strength of a pair of spur gears with machining errors, assembly errors and tooth modifications. Mech Mach Theory 42(1):88–114
26. Li S (2012) Contact stress and root stress analyses of thin-rimmed spur gears with inclined webs. J Mech Des 134(5):051001
27. Chang L, Liu G, Wu L (2015) A robust model for determining the mesh stiffness of cylindrical gears. Mech Mach Theory 87:93–114
28. Shweiki S, Rezayat A, Tamarozzi T, Mundo D (2019) Transmission error and strain analysis of lightweight gears by using a hybrid FE-analytical gear contact model. Mech Syst Signal Proc 123:573–590
29. Bathe K (2006) Finite element procedures. Prentice Hall, Hoboken
30. Lemke C (1965) Bimatrix equilibrium points and mathematical programming. Manage Sci 11(7):681–689
31. Lin T, He Z (2017) Analytical method for coupled transmission error of helical gear system with machining errors, assembly errors and tooth modification. Mech Syst Signal Proc 91:167–182
32. Dong H, Zhang C, Wang X, Wang D (2017) A precise FE model of a spur gear set considering eccentric error for quasi-static analysis. Mech Mach Sci 408:1263–1274
33. Gonzalez-Perez I, Roda-Casanova V, Fuentes A (2015) Modified geometry of spur gear drives for compensation of shaft deflections. Meccanica 50(7):1855–1867
34. Dong H, Zhang C, Bai S, Wang D (2019) Modeling, Analysis and testing of load distribution for planetary gear trains with 3D carrier pinhole position errors. Int J Precis Eng Manuf 20(8):1381–1394
35. Zhou C, Chen C, Gui L, Fan Z (2018) A nonlinear multi-point meshing model of spur gears for determining the face load factor. Mech Mach Theory 126:210–224
36. Peng Y, Zhao N, Qiu P, Zhang M, Li W, Zhou R (2018) An efficient model of load distribution for helical gears with modification and misalignment. Mech Mach Theory 121:151–168
37. StandardISO 6336–1 (2016) Calculation of load capacity of spur and helical gears, Part 1: basic principles, introduction and general influence factors. International Standard Organization, Geneva
38. Bruyere J, Velex P, Guilbert B, Houser DR (2019) An analytical study on the combination of profile relief and lead crown minimizing transmission error in narrow-faced helical gears. Mech Mach Theory 136:224–243
39. Sun Y, Ma H, Huangfu Y, Chen K, Che L, Wen B (2018) A revised time-varying mesh stiffness model of spur gear pairs with tooth modifications. Mech Mach Theory 129:261–278
40. Mohamad E, Komori M, Murakami H, Kubo A, Fang S (2009) Analysis of general characteristics of transmission error of gears with convex modification of tooth flank form considering elastic deformation under load. J Mech Des 13(6):2751–2764
41. Velex P, Maatar M (1996) A mathematical model for analyzing the influence of shape deviations and mounting errors on gear dynamic behavior. J Sound Vibr 191(5):629–660
42. Yu JC, Ishii K (1998) Design optimization for robustness using quadrature factorial models. Eng Optimiz 30:203–225
43. Artoni A, Guiggiani M, Kahraman A, Harianto J (2013) Robust optimization of cylindrical gear tooth surface modifications within ranges of torque and misalignments. J Mech Des 135(12):121005